

# Turbulence Modelling of Deep Dynamic Stall at Low Reynolds Number

Shengyi Wang, Lin Ma, Derek B Ingham, Mohamed Pourkashanian and Zhi Tao

**Abstract**—The unsteady separated turbulent flow around an oscillating airfoil pitching in a sinusoidal pattern in the regime of low Reynolds number is investigated numerically employing the *URANS* approach with two advanced turbulence models, namely the *RNG k-ε* model and Transition *SST* model, and the *DES* approach based on the *SST k-ω* model. A comparison with experimental data shows that the *SST k-ω* based *DES* approach is superior to the employed *URANS* turbulence models and presents good agreement with the validation data. The flow development of the dynamic stall is discussed.

**Key words**—*DES*, dynamic stall, low Reynolds number, *URANS*, wind turbine.

## I. INTRODUCTION

Dynamic stall has been widely known to significantly affect the performance of a large variety of fluid machinery, such as helicopter crafts, highly manoeuvrable fighters, gas turbines, and wind turbines. It has been well recognised that the dynamic stall process can be categorised into four key stages, i.e. attached flow at low angles of attack, development of the leading edge vortex (LEV), the shedding of the LEV from the suction surface of the blade and the reattachment of the flow [1]. Although the basic image of the phenomenon has been generally clarified, the physics of this strongly non linear unsteady flow phenomenon has not yet been completely understood and more efforts are needed to advance the knowledge to the level on which we could accurately predict and precisely control the dynamic stall [2]. Most of the previous researches have investigated flows at high Reynolds number ( $Re \geq 10^6$ ) or high Mach number ( $Ma \geq 0.3$ ) which fall into the compressible flow regime. However, dynamic stall at low Reynolds number has distinct features compared with those at high Reynolds number, such as flow transition process, laminar separation and reattachment, etc.

Manuscript received March 23, 2010. This work was supported in part by the Chinese Scholarship Council (CSC).

Mr. Shengyi Wang is a PhD student at the Beijing University of Aeronautics and Astronautics, Beijing, China and The University of Leeds, United Kingdom (phone: 44-113-3432569; fax: 44-113-2467310; e-mail: gmwsy@163.com or presw@leeds.ac.uk).

Dr. Lin Ma is at The University of Leeds, United Kingdom. (e-mail: L.Ma@leeds.ac.uk).

Professor Derek B Ingham is at The University of Leeds, United Kingdom. (e-mail: D.B.Ingham@leeds.ac.uk).

Professor Mohamed Pourkashanian is at The University of Leeds, United Kingdom. (e-mail: M.Pourkashanian@leeds.ac.uk).

Professor Zhi Tao is at Beijing University of Aeronautics and Astronautics, Beijing, China. (e-mail: tao\_zhi@buaa.edu.cn).

In the recent decades, due to the increased awareness of the environmental issues associated with the fossil fuel based power generation industry, wind industry is drawing more and more attention. Dynamic stall has been a critical phenomenon which has an important effect on the operation of both Horizontal Axis Wind Turbines (*HAWT*) and Vertical Axis Wind Turbines (*VAWT*). The aim of the present paper is to assess the ability of the Unsteady Reynolds-Averaged Navier-Stokes (*URANS*) method with two advanced turbulence models (*RNG k-ε* model and *Transition SST* model) [3] and the Detached Eddy Simulation (*DES*), in capturing the dynamic stall at low Reynolds number flows (Reynolds number based on the chord length of the airfoil  $Re_c$  is of the order of  $10^5$ ), and to provide a detailed two-dimensional analysis to gain a better understanding of the flow phenomenon.

## II. NUMERICAL SIMULATIONS

### A. Case studied

The airfoil employed in the numerical calculations is a NACA 0012 airfoil with a chord length of  $c=0.15m$ , which in this case executes the sinusoidal pitching motion  $\alpha=10^\circ+15^\circ \sin(18.67t)$  around an axis located at a quarter of its chord ( $0.25c$ ) from the leading edge with a reduced frequency  $k=\omega c/2U_\infty=0.10$ . The free stream velocity is  $U_\infty=14 m/s$  with a turbulence intensity of about 1% which corresponds to a chord Reynolds number of  $Re_c=1.35 \times 10^5$ . End plates were employed to minimize the flow leakage from the blade tip to reduce the 3D effects of the flow. A more comprehensive description of the experimental setup are detailed in [4].

### B. Numerical techniques

In this study, at first the simulations are performed using Unsteady Reynolds-Averaged Navier-Stokes (*URANS*) method. The reason is twofold: (1) *URANS* is numerically less expensive than Detached Eddy Simulation (*DES*); (2) The turbulence field obtained from the *URANS* results can be used as a guidance of the design of the grid for *DES*. The ANSYS Fluent 12.0 commercial solver is employed to solve the time-averaged (*URANS*) or space-averaged (the Large Eddy Simulation (*LES*) portion of the *DES* region) N-S equations.

#### 1) Grid design

##### a) Grid for the *URANS*

A typical C-grid as shown in Fig. 1 is used for the Unsteady *URANS* calculations. About 300 grid nodes are placed along the airfoil and they are clustered close to the

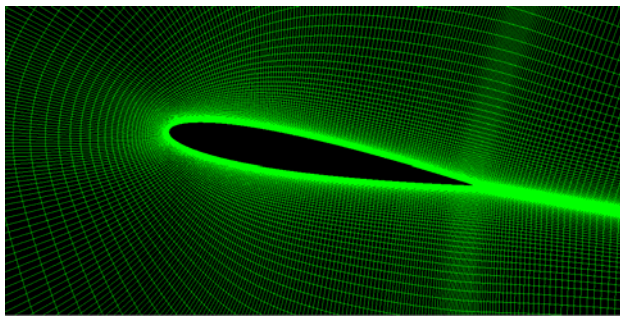


Figure 1 : C-type grid used for *URANS*.

leading and trailing edges. The height of the first row of cells of the cells bounding the airfoil is set to be  $10^{-5}c$  which ensures  $y^+ \leq 1.0$  for the cells immediately adjacent to the airfoil so that the boundary layer flow can be properly resolved without using a wall function. The height of the cells expands with a growth factor of 1.2 towards the external boundary which is set to be at  $20c$  from the airfoil to eliminate the boundary reflections. The whole mesh sums up to be 80,000. In order to simulate the sinusoidal pitching motion of the blade, the whole grid pitches like a rigid body with the same sinusoidal mode as the airfoil. This is achieved by using the dynamic mesh technique [3] with a User Defined Function (*UDF*) subroutine developed and attached to the ANSYS Fluent solver to control the movement of the grid points. The numerical time step size is set to be  $0.1T_c$  ( $T_c$  is the characteristic time which is equal to  $c/U_\infty$ ). Normally after three oscillation cycles, a perfect periodical solution can be obtained in this study.

b) *Grid for the DES*

The gridding for *DES* needs much more effort than that for *URANS* because the *LES* mode is activated in the non boundary layer regions where the grid size should be carefully chosen in order to capture the desirable portion of the turbulence kinetic energy (*TKE*). The flow field can be divided into three basic regions: Euler Region, RANS Region, and LES Region, of which the last two regions can be further divided into smaller regions [5], as shown in Table 1. Based on the *URANS* results, the flow field around the oscillating airfoil could be divided into several zones which are distinguished by different priorities in the grid spacing. Fig. [2] is the pressure field around the airfoil superimposed by the instant streamlines obtained from the *URANS* with the transitional *SST k- $\omega$*  model at the angle of attack of  $23.2^\circ$  during the upstroke phase ( $\alpha=23.2^\circ, \uparrow$ ) and it illustrates four of these regions; the viscous regions are too thin to sketch.

Table 1: Division of the flow field in *DES* [5].

Super-Region	Region
Euler (ER)	
RANS (RR)	Viscous (VR)
	Outer (OR)
LES (LR)	Viscous (VR)
	Focus (FR)
	Departure (DR)

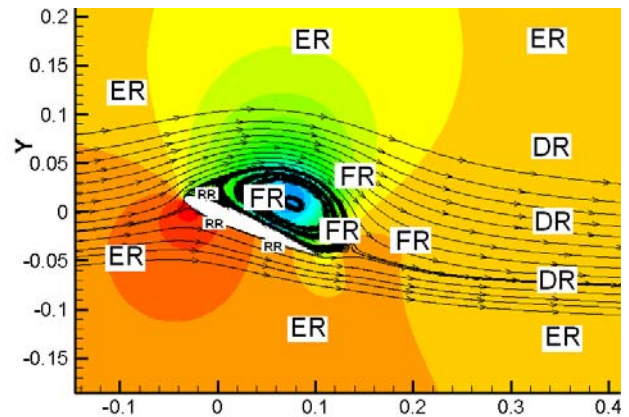


Figure 2: Sketch of the flow regions around an oscillating airfoil.

In RR, the grid requires a typical mesh for pure-RANS calculations and is the same as that discussed in section II.B.1)a). The FR is the most important part and the grid spacing determines the portion of *TKE* that can be captured by the simulations. In order to capture over 80% of the *TKE*, which is normally intended for *LES*, the grid spacing  $\Delta_0$  should be about 42% of the integral length scale  $l_0$ , as shown

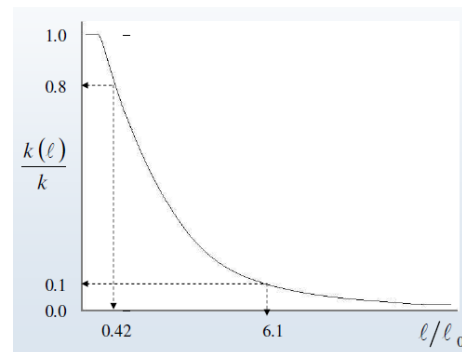


Figure 3: Cumulative *TKE* as a function of the integral length scale of the eddies based on the Kolmogorov's energy spectrum [6].

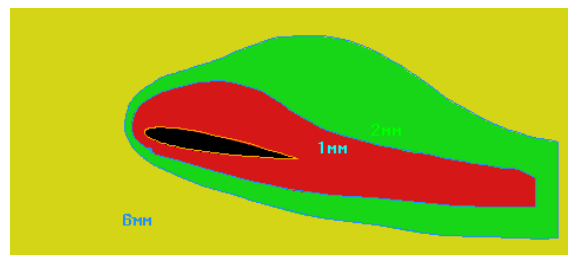
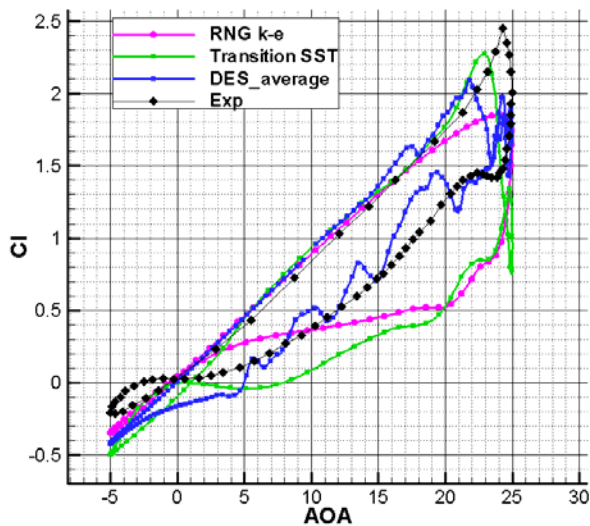
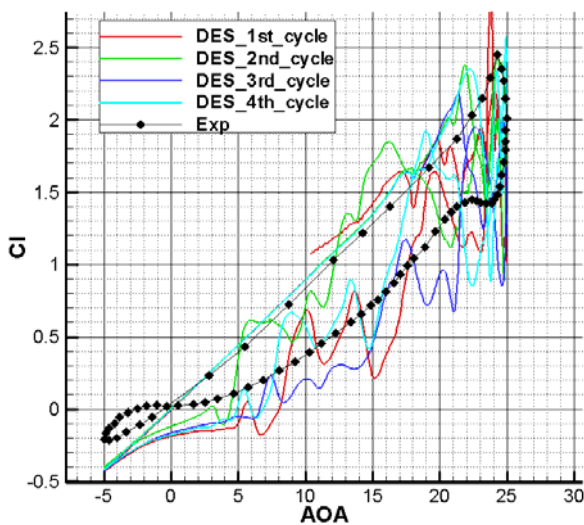


Figure 4: The distribution of the integral length scale around the oscillating airfoil.

in Fig. 3. In accordance with this rule, the field of  $l_0$  is estimated using the turbulence field obtained by *URANS*. Due to the oscillations of the blade, the turbulence field is always varying significantly for different values of  $\alpha$ , and therefore an estimation of the general situation of the turbulence field is gained by observing each field through each angle of attack. Fig. 4 shows the estimated distribution of  $l_0$ , on the basis of which the *DES* grid spacing is thus designed. The time step size is set to be  $0.039T_c$ , which corresponds to  $CFL \leq 5.9$  for the finest grid in the red region in Fig. 4.



(a) Comparison of the computed and experimental  $C_l$  hysteresis.



(b) Computed  $C_l$  hysteresis of the individual cycles using *DES*.

Figure 5: Computed and experimental  $C_l$  hysteresis for the deep dynamic stall of the NACA 0012 airfoil.

## 2) Turbulence models

### a) *RNG k-ε model*

The *RNG k-ε* model was derived using a rigorous statistical technique (called the renormalization group theory). Although it is similar in form to the standard *k-ε* model, it is modified such that the accuracy for rapidly strained flows and swirling flows has been significantly improved. In addition, the *RNG* theory provides an analytically-derived differential formula for the effective viscosity that accounts for the low *Re* effects.

### b) *Transition SST Model*

The transition *SST* Model is a four-equation turbulence model which is based on the coupling of the *SST k-ω* transport equations with two other transport equations, one for the intermittency and the other for the transition onset criteria, in terms of the momentum-thickness Reynolds number. This is a reasonably new model and it is expected to predict flows with massive separations more accurately. For further details on the transition *SST* Model, the reader is referred to [3].

### c) *SST k-ω based DES model*

*DES* is a recent approach which also is defined as a hybrid of *RANS* and *LES*, and it is aimed at accurately predicting separated flows [6]. In the *DES* approach, the unsteady *RANS* models are employed in the boundary layer while the *LES* treatment is applied in the separated regions outside of the boundary layer which are normally associated with the core turbulent region where large turbulence eddies play a dominant role. In this region, the *DES* model turns out to be a *LES*-like subgrid model. In the present study, the *DES model based on the SST k-ω* model is employed. The detailed formulation of the model can be found in [3].

## III. RESULTS AND DISCUSSIONS

### A. Numerical validation

Fig. 5(a) shows the computed sectional lift coefficient  $C_l$  obtained by using different turbulence modelling approaches, compared with the experimentally measured results [4]. It can be seen that for the portion with lower angle of attack during the upstroke phase, i.e.  $-5^\circ \leq \alpha \leq 18^\circ$ , all the models present satisfactory agreement with the experimental data. However, when  $(18^\circ \leq \alpha \leq 25^\circ)$ , the *RNG k-ε* model undershoots and diverges from the experimental data while the calculated value of  $C_l$  of the other two models have the same trend with the validation data. This is mainly because large flow separations occur when *AoA* is very large and the flow close to the suction surface of the airfoil becomes very complex. The stall of lift occurs later in the *Transition SST* model at  $\alpha \approx 23^\circ$  than at  $\alpha \approx 21^\circ$  in the averaged *DES* results. However, the *Transition SST* model presents too sharp a drop-off of the  $C_l$  when the lift stall occurs giving an over-prediction of the strength of the stall. The *DES* predictions, as shown in Fig. 5(b), show a very good consistence of  $C_l$  during the upstroke for low angles of attack, until  $\alpha \approx 18^\circ$ . For the rest portion of the upstroke phase, and most of the downstroke phase, the computed value of  $C_l$  presents a strong oscillating behaviour which implies the existence of intensive turbulence eddies due to the massive flow separations. In general, the prediction for the upstroke

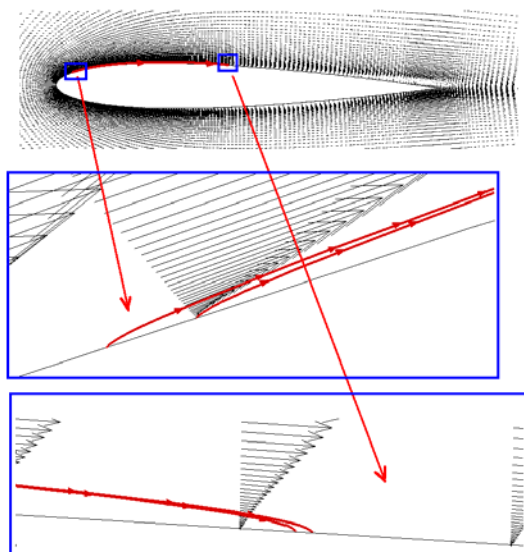


Figure 6: Demonstration of the thin separation layer.

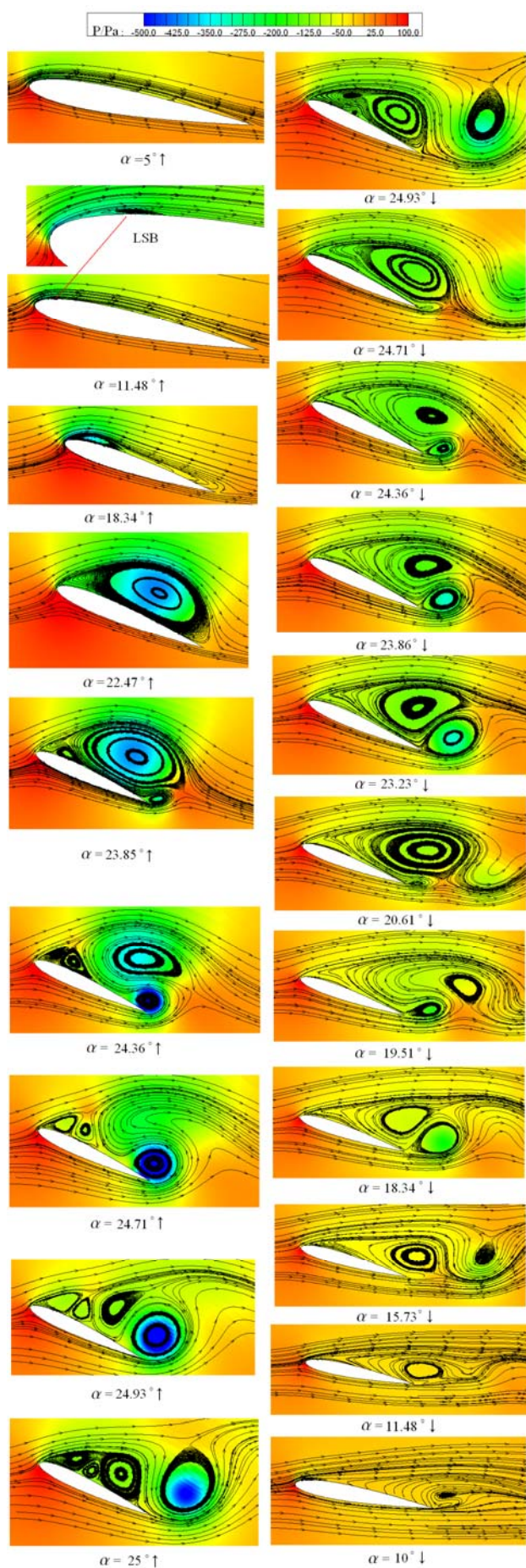


Figure 7: Pressure field superimposed on the instantaneous streamlines computed using the Transition SST model.

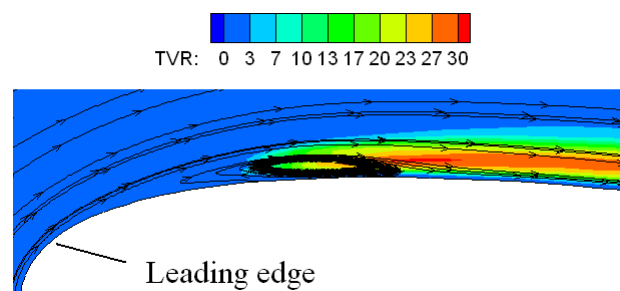


Figure 8: TVR field with the LSB.

phase is in fairly good agreement with the validation data in that the delay of the stall is captured reasonably well. In contrast with the upstroke phase, the prediction of the downstroke phase gained by the *URANS* models is not in good agreement with the experimental measurements due to the complicated post-stall flow structures. Since both the *RNG k-ε* model and the Transition *SST* model present a very sharp drop-off of the lift coefficient, the computed lift keeps below the measured lift line. Although the *DES* presents an unstable trend during the downstroke as illustrated in Fig. 5 (b), the averaged result presents a fairly good consistency with the validation data except for  $-5^\circ \leq \alpha \leq 5^\circ$ , see Fig.5 (a). This is probably due to its capacity of resolving the large eddies which play an important role in this period, while the modelling of the *URANS* models does not work well.

#### B. The dynamic stall process

Before discussing the flow development, it should be noted that due to the oscillating motion of the airfoil, the fluid particles adjacent to the airfoil should always have the same local velocities as that of the airfoil wall. In other words, there will always be instantaneous streamlines either starting from the airfoil surface or ending at it. Therefore, strictly speaking, there is no fully attached flow in this situation, even at very low angles of attack, for example  $\alpha \approx 0.5^\circ \uparrow$ , as shown in Fig. 6, even though the main flow is basically 'attached' the airfoil profile, there still exists a very thin separation layer due to the above-mentioned reason. However, as one can observe, this kind of separation is normally so thin that it does not affect the flow field and therefore, in this paper it is ignored and the flow shown in Fig. 6 is considered to be fully attached flow.

##### 1) Transition SST model

Dynamic stall is characterised by the process of the shedding of *LEV* which carries a low pressure wave that sweeps chord-wise across the suction surface of the airfoil. This feature, as can be seen in Fig. 7, is well captured by *URANS* with the Transition *SST* turbulence model. Fig.7 presents a chronology of the static pressure fields at different oscillating locations superimposed on the instantaneous streamlines to depict the complicated vortex structures during the stall process. In the early stage of the upstroke phase,  $-5^\circ \leq \alpha \leq 10^\circ$ , the flow is fully attached to the airfoil in the sense of ignoring the thin separation layer as in Fig. 6. At  $\alpha \approx 11.48^\circ$ , a tiny separation bubble can be detected close to the leading edge. Considering the low Reynolds number circumstances in this study, this bubble is actually the so-called Laminar Separation Bubble (LSB) in which the

flow turbulence intensity is significantly enhanced and this causes a turbulent boundary layer to appear after the LSB [7]. Fig. 8 shows the Turbulence Viscosity Ratio (TVR) field near the LSB at  $\alpha \approx 12.92^\circ \uparrow$ . As one can observe, the turbulence intensity is considerably increased after the LSB which forces a reattachment of the flow and this is a typical characteristic of the LSB. The LSB grows in size and travels towards the trailing edge of the airfoil as  $\alpha$  increases and at  $\alpha \approx 18.34^\circ \uparrow$  it has spanned about one third of the suction surface with a low pressure region around it. At this instance, the LSB has completely turned into the LEV. At  $\alpha \approx 22.47^\circ \uparrow$ , the LEV has covered the whole suction surface and  $C_l$  is at its maximum value, see Fig. 5. During the further convection of the LEV, it begins detaching from the airfoil surface and induces the trailing edge vortex due to the low pressure wave it carries and a pair of vortices at the leading edge, see  $\alpha \approx 23.85^\circ \uparrow$  and  $24.36^\circ \uparrow$ . The detachment of the LEV, as well as the flow separations due to the vortices it induces causes the value of  $C_l$  to decrease. At  $\alpha \approx 24.71^\circ \uparrow$ , the trailing edge vortex has grown and the LEV becomes very weak. However, the LEV appears to stop travelling down and forms another vortex between the trailing edge vortex and the leading edge vortex pair, as shown at  $\alpha \approx 24.93^\circ \uparrow$ . This point is very different from that obtained when using the traditional *SST k- $\omega$*  model by Wang, et al. [2]. At the maximum angle of attack, it turns out to be three vortices aligned alongside the suction surface. Then the airfoil comes to the downstroke phase. The vortices on the airfoil begin to emerge together and only one large vortex can be seen at  $\alpha \approx 24.71^\circ \downarrow$ . Similarly with the LEV, when this large vortex moves to the trailing edge, another trailing edge vortex is induced at  $\alpha \approx 24.36^\circ \downarrow$  and this becomes a large vortex at  $\alpha \approx 23.23^\circ \downarrow$ . Then a vortex shedding event, which is very similar to the Kármán Vortex Street, occurs: the trailing edge vortex sheds first followed by the shedding of the suction surface vortex. Then a second trailing edge vortex, which is generated by the just shedding suction surface vortex, grows large. After three pairs of vortices shed from the leading edge, at  $\alpha \approx 10^\circ \downarrow$ , the last vortex sheds and the flow begins to reattach with the airfoil.

### 2) RNG k- $\epsilon$ model

In contrast to the results obtained from the Transition *SST* model, the *RNG k- $\epsilon$*  model fails to achieve the LEV. The flow development is a simple story compared to that of the Transition *SST* model, as shown in Fig. 9. The flow can be considered as non-separated up to  $\alpha \approx 20.61^\circ \uparrow$ . A moderate separation can be seen from the trailing edge instead of the leading edge at  $\alpha \approx 23.37^\circ \uparrow$  and this spreads towards the leading edge smoothly. This may be because the *RNG k- $\epsilon$*  model is too dissipative to predict a severe adverse pressure gradient such that the LEV cannot be resolved properly. At  $\alpha \approx 25^\circ \uparrow$ , it has spanned the entire suction surface of the airfoil and as expected, a secondary trailing edge vortex is induced by the large separation. The reason why the *RNG k- $\epsilon$*  model underestimates the lift for  $18^\circ \leq \alpha \leq 25^\circ$  is that the separation does not originate from the LSB so that the vortex is merely a high pressure whirling flow. There is also a Kármán Vortex Street flow pattern during the downstroke phase.

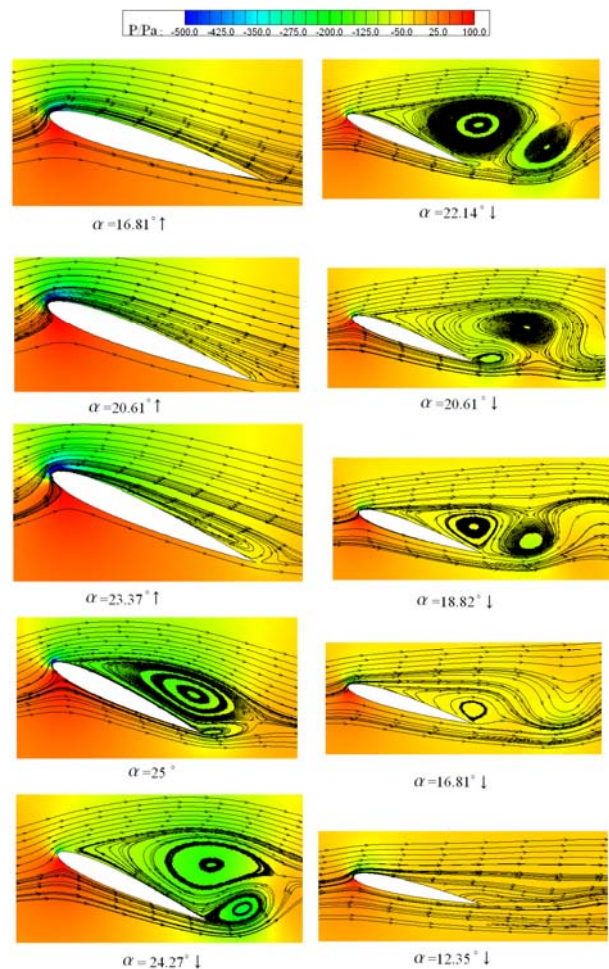


Figure 9: Pressure field superimposed on the instantaneous streamlines computed using the *RNG k- $\epsilon$*  model.

### 3) DES

As implied by the similarity of the computed value of  $C_l$  among the *DES* and *URANS* when the angles of attack are not high during the upstroke phase, the flow development of the *DES* is close to those of the *URANS*. Unlike the *URANS* simulations which can achieve an identical periodical solution normally from the third oscillation period, the flow details obtained from the *DES* differs from each other from cycle to cycle but the general flow patterns are similar. Hence the flow development during the third oscillation cycle is chosen to discuss below. The LSB occurs at  $\alpha \approx 14.64^\circ \uparrow$  which is later than in the Transition *SST* model. It should be noted that a trailing edge vortex forms at  $\alpha \approx 17.84^\circ \uparrow$ , which is not observed in the *URANS* simulations. Clearly it is not induced by the LEV. In addition, the secondary pair of leading edge vortices occurs much earlier and at  $\alpha \approx 21.41^\circ \uparrow$  it has grown to be almost as large as the LEV. However, it dissipates very quickly and becomes very weak at  $\alpha \approx 22.13^\circ \uparrow$ . The LEV separates from the airfoil at  $\alpha \approx 22.79^\circ \uparrow$  and this corresponds to the decrease in  $C_l$ . Because the shedding of the LEV occurs at a relatively low angle of attack, during the consequent upstroke of the airfoil, a series of vortices forms at the leading edge and travels along the suction surface of the airfoil. Since these vortices possess the local low pressure when they are generated at the leading edge, they actually act like the LEV but the strength is not as strong. The *DES* flow is much more complicated in

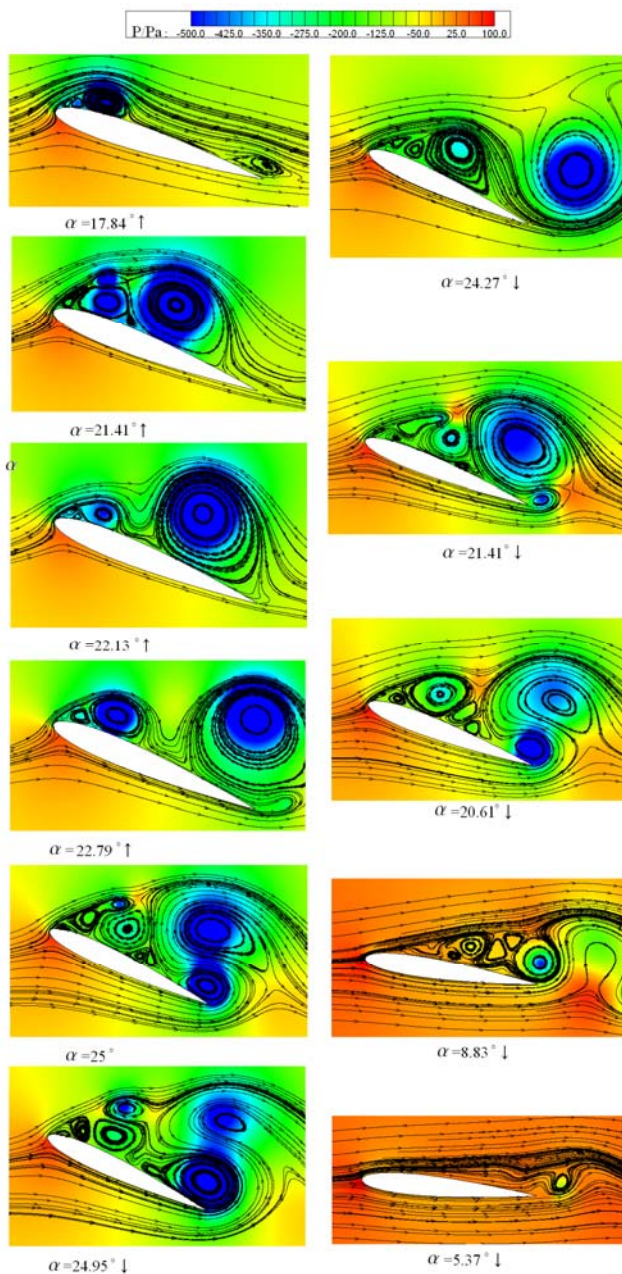


Figure 10: Pressure field superimposed on the instantaneous streamlines computed using  $k-\omega$  based *DES* model (Results from the third oscillation period).

that more details of the flow can be captured and this results in a more complex system of vortices. It can be deduced that it is the vortices which are produced continuously that cause the fluctuating behaviour of the computed  $C_l$ . It is considered unnecessary and too wordy to detail the flow development as several flow patterns extracted from the results during the third oscillation period have been presented in Fig. 10.

#### IV. CONCLUSIONS

In this paper, two RANS turbulence models, namely the *RNG*  $k-\epsilon$  model and the Transition *SST* model, and the *SST*  $k-\omega$  based *DES* model have been employed to simulate the fluid flow around a NACA 0012 airfoil executing a sinusoidal pitching, in the low Reynolds number fluid flow regime. In general, all the turbulence models employed can predict the experimental data with reasonable accuracy, except at very high angles of attack where massive flow

separations are encountered and the hysteresis loop of the lift coefficients has been clearly obtained. It can be concluded that the Transition *SST* model is capable of predicting the flow characteristics for the upstroke phase while the main difficulty lies in the accurate modelling of the complicated separated flows during the downstroke phase. In this study, the *SST*  $k-\omega$  based *DES* model presents good agreement with the experimental data especially for the downstroke phase where the Transition *SST* model fails.

#### ACKNOWLEDGMENT

The authors would like to acknowledge the financial support from the Chinese Scholarship Council (CSC) for this research. Also the authors would like to express their gratitude to Professor T. Lee from McGill University, Canada, for offering useful information and constructive comments on the experiment studies this paper.

#### REFERENCES

- [1] P. Wernert, W. Geissler, M. Raffel, and J. Kompenhans, "Experimental and numerical investigations of dynamic stall on a pitching airfoil," *AIAA journal*, vol. 34, pp. 982-989, 1996.
- [2] S. Wang, L. Ma, D. Ingham, M. Pourkashanian, and Z. Tao, "Numerical Investigations on Dynamic Stall Associated with Low Reynolds Number Flows over Airfoils," in *The 2010 International Conference On Mechanical and Aerospace Engineering (CMAE 2010)* Chengdu, China, 2010.
- [3] ANSYS Inc, "ANSYS FLUENT 12.0 (Theory Guide)," 2009.
- [4] T. Lee and P. Gerontakos, "Investigation of flow over an oscillating airfoil," *J FLUID MECH*, vol. 512, pp. 313-341, 2004.
- [5] P. R. Spalart, "Young-person's guide to Detached-Eddy Simulation grids," 2001.
- [6] G. Aleksey, "LES & DES in FLUENT," *ANSYS training material*, 2007.
- [7] P. R. Spalart, "Strategies for turbulence modelling and simulations," vol. 21: Elsevier, 2000, pp. 252-263.
- [8] P. Spalart, "Strategies for turbulence modelling and simulations," *International Journal of Heat and Fluid Flow*, vol. 21, pp. 252-263, 2000.